tively, it was interesting to study the interaction of HN_3 with both the N_3^- and the F^- anions. With $N(CH_3)_4N_3$, HN_3 did not form an adduct stable at room temperature. With MF [M = Na, K, Rb, Cs, $N(CH_3)_4$], gaseous or liquid HN_3 reacted at or below room temperature with the formation of an equimolar mixture of MN_3 and MHF_2 (4). The products of reaction 4 are best

$$2MF + HN_3 \rightarrow MN_3 + MHF_2 \quad (4)$$

interpreted by the summation of (5) and (6), where step 5 might

$$MF + HN_3 \rightarrow MN_3 + HF \quad (5)$$

$$MF + HF \rightarrow MHF_2 \quad (6)$$

involve an intermediate $F-H-N_3^-$ anion which readily eliminates HF to give the final N_3^- product. Attempts were made to isolate this intermediate anion by reacting HN_3 with a RbF single crystal infrared window at low temperature. Below -100 °C, no reaction occurred, and above this temperature, the only new products observable by infrared spectroscopy were RbN_3 and $RbHF_2$.

Reaction 5, i.e. the displacement of F^- from M^+F^- by HN_3, was surprising since, in aqueous solution, HN_3 (P_k = 4.77) is a weaker acid than HF (P_k = 3.18). Furthermore, molten weak organic acids such as stearic acid also displace N_3^- from NaN_3.[8] Since reaction 5 was not carried out in aqueous solution in which the acidity of HF is enhanced by the hydration energy of F^-, but between solid MF and neat gaseous or liquid HN_3, it should not be governed by the above P_k values but by the proton affinities of F^- and N_3^-. In view of the proton affinity of F^- (371.5 kcal mol^{-1}) exceeding that of N_3^- (328.6 kcal mol^{-1}) by about 43 kcal mol^{-1}, it is then not surprising that HN_3 can displace F^- from M^+F^-.

On the other hand it was found that HF quantitatively displaces N_3^- from $M^+N_3^-$ (7). This reaction does not require the use of an excess of HF. If less than the stoichiometric amounts of HF are used, the resulting products still are MHF_2 and HN_3 and not MF and HN_3. Hence, it appears that both reactions 5 and 7 are

$$MN_3 + 2HF \rightarrow MHF_2 + HN_3 \quad (7)$$
$$M = Na, Cs, N(CH_3)_4$$

irreversible and that the puzzling observations that HN_3 displaces F^- from MF (5) while HF displaces N_3^- from MN_3 (7) are not due to the shifting of a single chemical equilibrium (8).

$$MF + HN_3 \rightleftarrows MN_3 + HF \quad (8)$$

The observed reaction chemistry can be explained by the vastly different Lewis basicities of F^- and HF_2^-. Thus, the very strong Lewis base F^- is readily displaced by the weak acid HN_3 (5), but the more acidic HF_2^- anion is the final product which, once it has been formed, cannot be displaced anymore by the weak acid HN_3.

Acknowledgment. We thank C. J. Schack and R. D. Wilson for their help and the U.S. Air Force Phillips Laboratory and the U.S. Army Research Office for financial support of the work carried out at Rocketdyne.

Registry No. Trimethylsilyl azide, 4648-54-8; tetramethylammonium fluoride, 373-68-2; tetramethylammonium azide, 999-77-9; hydrazoic acid, 7782-79-8; sodium fluoride, 7681-49-4; potassium fluoride, 7789-23-3; rubidium fluoride, 13446-74-7; cesium fluoride, 13400-13-0; azide, 14343-69-2; bifluoride, 18130-74-0; fluoride, 16984-48-8; hydrogen fluoride, 7664-39-3.

Supplementary Material Available: Tables of final atomic coordinates and anisotropic thermal parameters (2 pages); tables of calculated and observed structure factor amplitudes (2 pages). Ordering information is given on any current masthead page.

(24) Al-Zamil, N. S.; Evans, E. H. M.; Gillard, R. D.; James, D. W.; Jenkins, T. E.; Lancashire, R. J.; Williams, P. A. *Polyhedron* **1982**, *1*, 525.
(25) Roziére, J.; Lehman, M. S.; Potier, J. *Acta Crystallogr.* **1979**, *B35*, 1099.
(26) Roziére, J.; Roziére-Bories, M. T.; Williams, J. M. *Inorg. Chem.* **1976**, *15*, 2490.
(27) Williams, J. M.; Dowling, N.; Gunde, R.; Hadzi, D.; Orel, B. *J. Am. Chem. Soc.* **1976**, *98*, 1581.
(28) Roziére, J.; Berney, C. V. *J. Am. Chem. Soc.* **1976**, *98*, 1582.
(29) Al-Zamil, N.; Delf, B. W.; Gillard, R. D. *J. Inorg. Nucl. Chem.* **1980**, *42*, 1117.
(30) Karelin, A. I.; Grigorovich, Z. I.; Rosolovskii, V. Ya. *Izv. Akad. Nauk. SSSR, Ser. Khim.* **1974**, 1228.

Formation of Fibrous Molecular Assemblies by Amino Acid Surfactants in Water

Toyoko Imae,* Yoshiyuki Takahashi, and Hidetoshi Muramatsu

Contribution from the Department of Chemistry, Faculty of Science, Nagoya University, Nagoya 464, Japan. *Received May 9, 1991. Revised Manuscript Received December 9, 1991*

Abstract: Gel-like solutions are obtained at medium pH and low temperature for aqueous solutions of *N*-acyl-L-aspartic acids (C_nAsp, n = 12-18). Electron microscopic observation reveals that helical, fibrous molecular assemblies are formed in the gel-like solutions. The rheological behavior reflects the formation of swarms or bundles of fibers. The hydrogen bonding of amide groups and the moderate degree of ionization of carboxyl groups are confirmed from the infrared absorption bands, consistent with the pH titration result. The possible models of helical, fibrous assemblies are the double stranded or the superhelical structure of helical bilayer strands or the twisted ribbon of a planar bilayer sheet. While *N*-dodecanoyl-L-glutamic acid (C_{12}Glu) molecules cannot be associated into fibrous assemblies, *N*-dodecanoyl-β-alanine (C_{12}Ala) molecules form cylindrical fibers which have no helical structure.

Biopolymers such as polynucleotides, polypeptides, and polysaccharides can take the helical structure which is very important in the occurrence of biological functions. The formation of similar helical structures has recently been reported for assemblies of some native and artificial amphiphiles.

When mineral oil was used as a dispersion medium, lithium 12-hydroxystearate formed fibers with the structure of a twisted ribbon or helical rope.[1] Twisted fibrous aggregates were also constructed by *N*-(2-hydroxydodecyl) amino acids in organic solvents.[2] Helical and cylindrical aggregates in an aqueous

(1) Tachibana, T.; Kambara, H. *J. Am. Chem. Soc.* **1965**, *87*, 3015-3016.
(2) Hidaka, H.; Murata, M.; Onai, T. *J. Chem. Soc., Chem. Commun.* **1984**, 562-564.

0002-7863/92/1514-3414$03.00/0

medium were reported for deoxycholic acid,[3,4] mixtures of acid phospholipids and phosphatidylcholines in the presence of Ca^{2+},[5] synthetic amphiphiles with a rigid segment,[6-8] 5′-phosphatidyl nucleosides,[9,10] ethanolamine-type phospholipids,[11] alkylaldonamides,[12-14] and D-dodecyltartaric amide monocarboxylate.[15]

The hydrophobic interaction between long hydrocarbon chain moieties in amphiphiles is essential in the supermolecular aggregation, and the interaction between head groups is a possible driving force for the formation of helical and/or cylindrical aggregates.[2,4,7,12-14] On the other hand, the chirality of amphiphilic molecules dominates the helical structure.[1,2,4,7,12]

Since *N*-acyl amino acids are surfactants with a long hydrocarbon chain and amide and carboxyl functional groups, the formation of fibrous assemblies can be expected for this kind of amphiphiles. In this work, the construction of such assemblies is investigated for aqueous solutions of a group of amino acid surfactants, *N*-acyl-L-aspartic acids (C_nAsp), and possible molecular arrangements are discussed for fibrous assemblies. Moreover, the assembly formation is compared with that of other analogous amino acid surfactants, *N*-(2-hydroxydodecyl)-L-aspartic acid (C_{12}HAsp), *N*-dodecanoyl-L-glutamic acid (C_{12}Glu), and *N*-dodecanoyl-β-alanine (C_{12}Ala), and the effect of the hydrophilic moiety is examined.

C_nAsp: $C_{n-1}H_{2n-1}CNHCHCOOH$ (n = 10, 12, 14, 16, 18)
(O; CH_2COOH)

C_{12}HAsp: $C_{10}H_{21}CHCH_2NHCHCOOH$
(OH; CH_2COOH)

C_{12}Glu: $C_{11}H_{23}CNHCHCOOH$
(O; CH_2CH_2COOH)

C_{12}Ala: $C_{11}H_{23}CNHCH_2CH_2COOH$
(O)

Results and Discussion

pH Titration Curves and Phase Diagrams of Aqueous C_nAsp Solutions. Figure 1 illustrates the degree of ionization α at room temperature as a function of pH for aqueous solutions of C_nAsp (n = 12, 14, 16, 18) at a surfactant concentration of 10^{-3} g cm^{-3}. The degree of ionization changes sharply at a certain pH, and the titration curve shifts to higher pH with increasing hydrocarbon chain length.

While the titration curves of C_nAsp, n = 12, 14, 16, present one inflection, that of C_{18}Asp reveals two inflections. Since similar behavior is observed for aqueous solutions of fatty acids[16] besides those of amphiphiles with dicarboxyl polar groups,[17,18] the two-step transition does not originate with dicarboxyl amphiphiles. It is suggested that the titration curves of mono- and dicarboxyl amphiphiles might be concerned with the hydrolysis of carboxylate and the resultant phase transition, such as the formation of fine crystals or vesicles.[17-20] The aqueous C_nAsp solutions may be such a case.

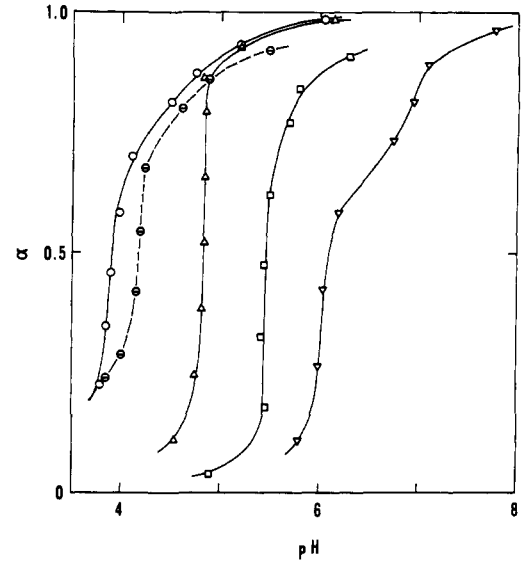

Figure 1. Degree of ionization α as a function of pH for aqueous solutions of 10^{-3} g cm^{-3} C_nAsp and C_{12}Glu at room temperature: ○, C_{12}Asp; △, C_{14}Asp; □, C_{16}Asp; ▽, C_{18}Asp; ⊖, C_{12}Glu.

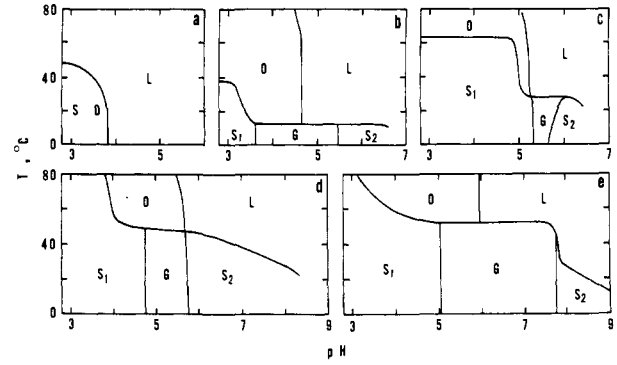

Figure 2. Temperature–pH phase diagrams for aqueous C_nAsp solutions of 1%: (a) C_{10}Asp; (b) C_{12}Asp; (c) C_{14}Asp; (d) C_{16}Asp; (e) C_{18}Asp. Notation: L, transparent; O, opalescent; S, S_1, S_2, solid; G, gel-like.

Table I. Assembly Formation by Amino Acid Amphiphiles

amphiphiles	pH	temp (°C)	solution property	morphology
C_{10}Asp	<3.8	<48	opalescent	vesicle
C_{12}Asp	<4.7	>12	opalescent	vesicle
	3.6–5.5	<12	gel-like	helical fiber
C_{14}Asp	<5.2	>27	opalescent	vesicle
	5.3–6.0	<28	gel-like	helical fiber
C_{16}Asp	<5.7	>47	opalescent	vesicle
	4.7–5.8	<50	gel-like	helical fiber
C_{18}Asp	<6.0	>52	opalescent	vesicle
	5.0–7.7	<52	gel-like	helical fiber
C_{12}Glu	<4.9	low	gel	gel
C_{12}Ala	<5.7	high	opalescent	
	<6	low	cylindrical	cylindrical fiber

Figure 2 gives the temperature–pH phase diagrams for aqueous C_nAsp solutions at a concentration of 1% (g/100 cm^{-3} solvent). Although aqueous C_{10}Asp solutions are transparent at high tem-

(3) McCrea, J. F.; Angerer, S. *Biochem. Biophys. Acta* **1960**, *42*, 357–359.
(4) Ramanathan, N.; Currie, A. L.; Colvin, J. R. *Nature* **1961**, *190*, 779–781.
(5) Lin, K.-C.; Weis, R. M.; McConnell, H. M. *Nature* **1982**, *296*, 164–165.
(6) Kunitake, T.; Okahata, Y.; Shimomura, M.; Yasunami, S.; Takarabe, K. *J. Am. Chem. Soc.* **1981**, *103*, 5401–5413.
(7) Nakashima, N.; Asakuma, S.; Kim, J.-M.; Kunitake, T. *Chem. Lett.* **1984**, 1709–1712.
(8) Kunitake, T.; Yamada, N. *J. Chem. Soc., Chem. Commun.* **1986**, 655–656.
(9) Yanagawa, H.; Ogawa, Y.; Furuta, H.; Tsuno, K. *Chem. Lett.* **1988**, 269–272.
(10) Yanagawa, H.; Ogawa, Y.; Furuta, H.; Tsuno, K. *J. Am. Chem. Soc.* **1989**, *111*, 4567–4570.
(11) Takeoka, S.; Sakai, H.; Iwai, H.; Ohno, H.; Tsuchida, E. *Polym. Prepr., Jpn.* **1989**, *38*, 568.
(12) Fuhrhop, J.-H.; Schnieder, P.; Rosenberg, J.; Boekema, E. *J. Am. Chem. Soc.* **1987**, *109*, 3387–3390.
(13) Fuhrhop, J.-H.; Schnieder P.; Boekema, E.; Helfrich, W. *J. Am. Chem. Soc.* **1988**, *110*, 2861–2867.
(14) Fuhrhop, J.-H.; Demoulin, C.; Rosenberg, J.; Boettcher, C. *J. Am. Chem. Soc.* **1990**, *112*, 2827–2829.
(15) Fuhrhop, J.-H.; Svenson, S.; Boettcher, C.; Rossler, E.; Vieth, H.-M. *J. Am. Chem. Soc.* **1990**, *112*, 4307–4312.
(16) Feinstein, M. E.; Rosano, H. L. *J. Phys. Chem.* **1969**, *73*, 601–607.
(17) Imae, T.; Suzuki, S.; Abe, A.; Ikeda, S.; Fukui, Y.; Senoh, M.; Tsujii, K. *Colloids Surf.* **1988**, *33*, 75–83.
(18) Nakazawa, K. M.Sc. Thesis, Nagoya University, Nagoya, Japan, 1991.
(19) Hargreaves, M. R.; Deamer, D. W. *Biochemistry* **1978**, *17*, 3759–3768.
(20) Cistola, D. P.; Atkinson, D.; Hamilton, J. A.; Small, D. M. *Biochemistry* **1986**, *25*, 2804–2812.

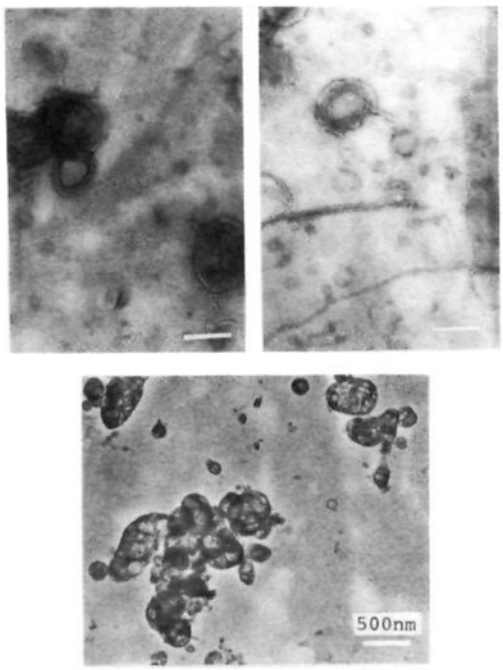

Figure 3. Electron micrographs from an opalescent C_{12}Asp solution of 1% at pH 3.32: upper, negative staining; lower, cryo. The bars represent 500 nm.

perature and pH, the solutions at less than 48 °C present opalescence below pH 3.8 and precipitate at lower pH.

Five separate regions are obvious for aqueous solutions of C_nAsp (n = 12, 14, 16, 18). At higher temperatures, the transparent solutions are observed at alkaline pH and the opalescent solutions occur at acid pH. At lower temperatures, while there are two solid regions at acid and alkaline pH, a viscous, gel-like region appears between them. The solid and gel-like regions shift to higher temperatures with increasing hydrocarbon chain length of surfactant, reflecting the chain length dependence of the Krafft point and, therefore, the hydrophobic interaction between hydrocarbon chains.

The pH and temperature regions of opalescent and gel-like solutions of C_nAsp are listed in Table I with the morphology of assemblies in the solutions which is presented later. The opalescent and gel-like regions shift to higher pH with increasing hydrocarbon chain length of the surfactant. This fact is consistent with the shifting tendency on the titration curves, suggesting the relationships between the phase regions and the degree of ionization: the opalescent solutions belong to the carboxyl-rich region, and the gel-like solutions are in the transition region between carboxyl and carboxylate species.

When the concentration of C_{14}Asp is varied from 0.5 to 4%, the phase diagrams are very similar, except that the opalescent region extends down to 33 °C at 4%.

Microscopic Observation of Aqueous C_nAsp Solutions. When optical microscopic observations are carried out for the opalescent C_nAsp solutions, numerous spherical particles with various diameters are observed, while such particles are invisible in the transparent solutions. The gel-like solutions present swarms which seem to be formed by numerous fine particles. The precipitates in the solid regions are mainly needle-like crystals, and those in the two different solid regions of acid and alkaline pH are indistinguishable by optical microscopic observation.

Figure 3 shows electron micrographs of specimens prepared from an opalescent C_{12}Asp solution of 1% at pH 3.32. There are images of vesicle-like spherical particles with membrane layers in the photographs from a negative staining method and images of large particles encapsulating small particles in one of the photographs from a cryo method. The particles are of different sizes less than 500 nm.

The video-enhanced differential interference contrast microscopic (VEM) observation was carried out for opalescent (translucent) solutions of C_{14}Asp at medium pH.[21] Vesicles with diameters of less than 7 μm coexisted with smaller particles. Although it is difficult to observe the fine structure of small particles by a VEM technique, small particles can be identified as small vesicles on the basis of the present work.

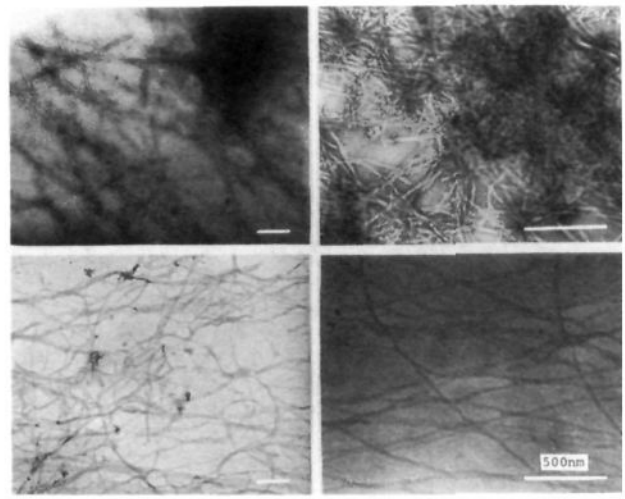

Figure 4. Electron micrographs from a gel-like C_{14}Asp solution of 1% at pH 5.05: upper, negative staining; lower, cryo. The bars represent 500 nm.

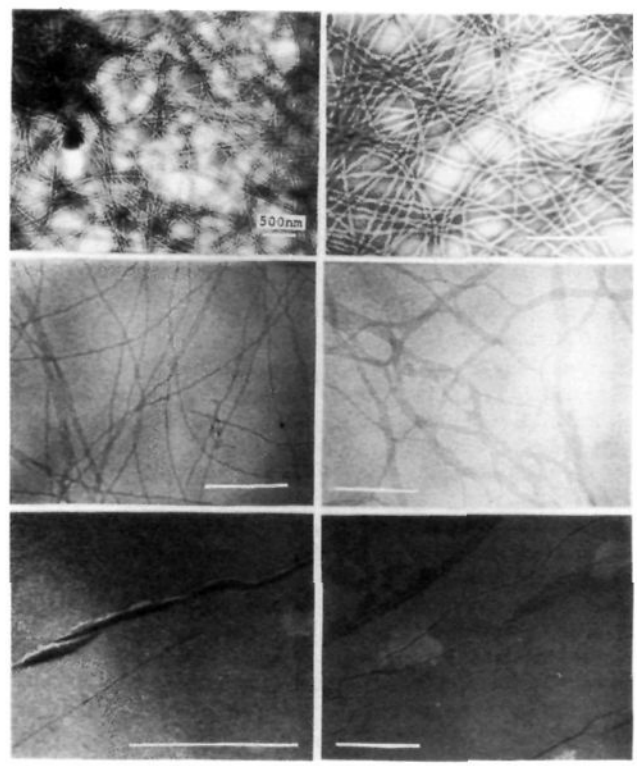

Figure 5. Electron micrographs from a gel-like C_{16}Asp solution of 1% at pH 5.17 or 5.77: upper, negative staining (pH 5.17); middle, cryo (pH 5.17); lower, freeze–fracture (pH 5.77). The bars represent 500 nm.

The electron micrographs from gel-like solutions of 1% C_{14}Asp and 1% C_{16}Asp at pH 5.05 and 5.17 or 5.77, respectively, are given in Figures 4 and 5. The fibrous images are evident in all photographs. The fibers have a uniform, common diameter of about 12–20 nm when it is estimated from photographs by the cryo and freeze–fracture methods, although the diameter from a negative staining method is somewhat larger due to artifacts caused by its preparation. The diameter is 4–7 times thicker than the theoretical molecular length of amphiphile with the trans, zigzag hydrocarbon

(21) Imae, T.; Trend, B. *Langmuir* **1991**, *7*, 643–646.

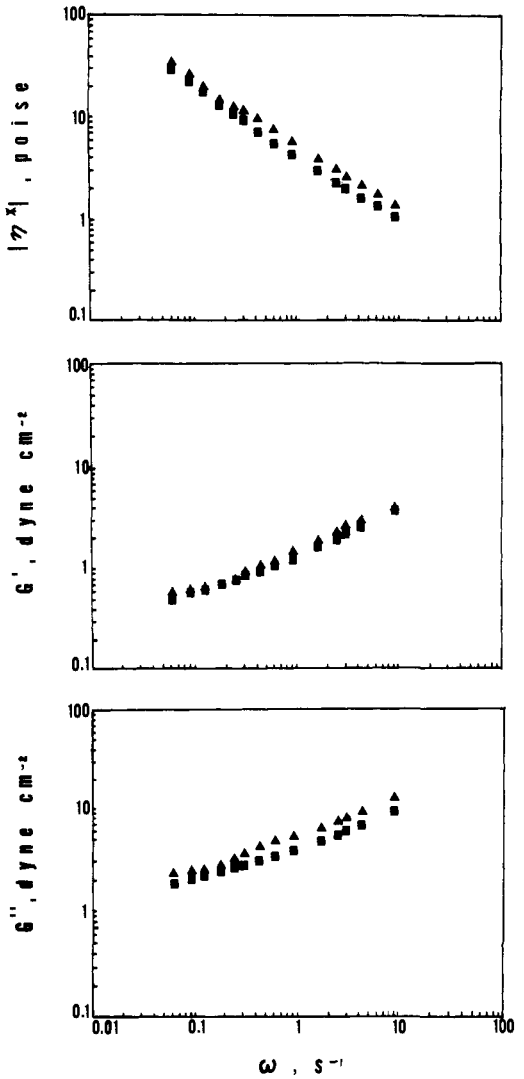

Figure 6. Absolute complex viscosity and storage and loss moduli as a function of angular frequency for gel-like C_{16}Asp solutions of 1 wt % at 25 °C: ▲, pH 5.37; ■, pH 5.66.

chain configuration, suggesting that the fibrous assemblies are not rodlike micelles.

The fibers are too long to find an individual string. They are slightly flexible and have a twisted or helical conformation with a helical pitch of about 65 nm. The fibers arrange in a parallel manner in terms of the side-by-side interaction, implying the formation of bundles and/or parallel sheets. On the other hand, as seen in the right, upper photograph of Figure 4, fibers can make a "mass" in which the fibers are concentrated and packed. It can be inferred that "masses" seem to be swarms in optical microscopy. Even if one end of a fiber is included in a "mass", the other end may be included in another "mass" or be dispersed in the bulk solution. The formation of swarms and/or bundles of fibrous assemblies may cause viscous and sometimes viscoelastic properties.

Rheological and Spectroscopic Measurements of Aqueous C_nAsp Solutions. The absolute complex viscosity, $|\eta^*|$, the storage modulus, G', and the loss modulus, G'', for gel-like C_{16}Asp solutions of 1 wt % (g/100 g solution) at 25 °C are plotted as a function of angular frequency ω in Figure 6. Those at pH 5.37 and 5.66 have no remarkable difference. The complex viscosity and the storage and loss moduli, respectively, decrease and increase gradually with an increse in angular frequency, and the slopes of the moduli as a function of angular frequency are more gradual than those estimated for a Maxwell fluid. This feature is different from the rheological results for entangled, long rodlike micelles,[22,23]

(22) Hashimoto, K.; Imae, T. *Langmuir* **1991**, *7*, 1734–1741.

Table II. Infrared Absorption Bands and Their Assignments

C_{16}Asp	α-PGA[a]	α-SPG[a]	soap[b]	assignment
3308 s				amide A
2924 s				CH_2 antisym str
2858 s				CH_2 sym str
1700–1710 m	1705			C=O str (COOH)
1645 s	1650	1645		amide I
~1570 sh		1570	1560	COO^- antisym str
1530–1550 s	1550	1545		amide II
1470 m			1460	CH_2 sym bend. def
1415 m		1408	1415	COO^- sym str
1391 sh			1380	CH_3 sym bend. def
1305 sh }				O–H def + C–O str (COOH)
1289 m }				amide III

[a] From ref 28. [b] From ref 29.

but it is similar to characteristics of the gelatinous linear polymer solutions, where the bundle structure of polymer chains is formed.[24-27] The formation of swarms or bundles of fibrous C_nAsp assemblies, which is confirmed by the electron micrographs, gives rise to the storage of internal energy and the rheological properties with the complicated multirelaxation mechanism.

The infrared spectrum was measured for the dried specimen prepared from a gel-like C_{16}Asp solution of 1 wt % at pH 5.82 and room temperature. On the process of drying, there are not any significant frequency shifts and intensity changes of the absorption bands, except the diminution of the band intensity of water. Although the specimen dried in air was further dried in vacuo in a desiccator with silica gel, the spectrum scarcely changed.

The assignments of the absorption bands are listed in Table II, where the bands are compared with those of α-helical poly-L-glutamic acid (α-PGA), α-helical sodium poly-L-glutamate (α-SPG),[28] and anhydrous sodium soaps (soap).[29] A 3308 cm^{-1} band can be assigned to the amide A (hydrogen-bonded NH stretching) vibration mode, and the amide I (1645 cm^{-1}) and II (1530–1550 cm^{-1}) modes are consistent with those of α-PGA and α-SPG. This suggests that the amide groups are hydrogen-bonded, and their arrangement in the helical structure of C_nAsp fibers may be similar to that in the α-helical structure of polypeptides. It is obvious from the existence of 1700–1710, ~1570, and 1415 cm^{-1} bands that the carboxyl and carboxylate species coexist in helical C_{16}Asp fibers. This is consistent with the result from the pH titration and the phase diagram that the gel-like solutions are in the transition region between the carboxyl and carboxylate species.

When the gel-like C_{16}Asp solutions are prepared, the solutions must first pass through an opalescent state: they are maintained for more than 2 h at 60–80 °C before their temperature is lowered to 25 °C. If the solutions at high temperature are immediately cooled down, precipitates form. When the precipitated solutions are aged through the heating process, one can obtain the opalescent vesicle solutions, which are also reproducible by heating the gel-like solutions. The gel-like C_{16}Asp solutions transform into gels or occasionally precipitates when left for a long period at room temperature. These results suggest that both the gel-like and opalescent solutions are in a metastable state and that the transformation between them may be explained as a gel–liquid crystal phase transition.

Possible Models of Helical C_nAsp Fibers. C_nAsp molecules form vesicles with bilayer membranes in acidic aqueous medium, if solutions are aged more than 2 h at high temperature. Vesicles in opalescent solutions at medium pH transform into fibers with decreasing temperature. While the transformation between vesicles and fibers is temperature-reversible, the gel-like fiber

(23) Hashimoto, K.; Imae, T.; Nakazawa, K. *Colloid Polym. Sci.*, in press.
(24) Rees, D. A. *Adv. Carbohydr. Chem. Biochem.* **1969**, *24*, 267–332.
(25) Morris, E. R.; Rees, D. A. *J. Mol. Biol.* **1980**, *138*, 363–374.
(26) McEvoy, H.; Ross-Murphy, S. B.; Clark, A. H. *Polymer* **1985**, *26*, 1483–1492.
(27) Burchard, W. *Br. Polym. J.* **1985**, *17*, 154–163.
(28) Lenormant, H.; Baudras, A.; Blout, E. R. *J. Am. Chem. Soc.* **1958**, *80*, 6191–6195.
(29) Chapman, D. *J. Chem. Soc.* **1958**, *152*, 784–789.

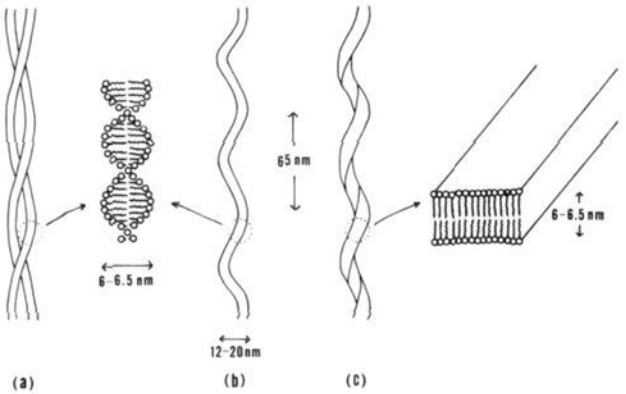

Figure 7. Possible models of C_nAsp fibers: (a) double strand of helical bilayer strands; (b) superhelical structure of a helical bilayer strand; (c) twisted ribbon of a planar bilayer sheet.

solutions are metastable as are the opalescent vesicle solutions and shift to gels or form precipitates in the course of time. Fibrous C_nAsp assemblies have a uniform, common diameter and are very long. Slightly flexible twisted fibers make masses or contact by the side-by-side interaction.

Recently, two plausible molecular models of the helical structure were proposed. One is a helical bilayer strand structure where linear bilayers twist.[10,12] The helical strands can form a superhelical structure or they may form double strands which, in turn, arrange in a superhelical structure. The other model is a twisted ribbon structure which is constructed by twisting planar bilayer sheets.[13] The rolling up of the planar bilayer sheets yields tubes or cigarlike scrolls.

The possible models of helical C_nAsp fibers are illustrated in Figure 7. In constructing these models, we consider the fact that the diameter and pitch of C_nAsp fibers are 12–20 nm and 65 nm, respectively. The models are, respectively, the double strand of helical bilayer strands, the superhelical structure of a helical bilayer strand, and the twisted ribbon of a planar bilayer sheet. All three of these models are plausible. Bilayers arrange by the hydrophobic interaction between hydrocarbon chains. The hydrogen bonding between amide groups strengthens such bilayer arrangements, and the chirality of the asymmetric carbon demands the helical structure of bilayer strands or the twist of ribbons. The coexisting carboxyl and carboxylate groups may reinforce the fibrous structure by intrafiber hydrogen bonding such as $COO^-\cdots HOOC$. Alternatively, they may cause the interfiber hydrogen-bonding interaction which induces the double strand, the swarm, or the bundle formation of C_nAsp fibers and, therefore, the viscous and viscoelastic behavior of gel-like solutions.

Formation of Molecular Assemblies by C_{12}HAsp. Above pH 5.6, C_{12}HAsp solids dissolve in water and generate opalescent solutions, while the solids at low pH are insoluble in water. C_{12}HAsp molecules are less soluble than C_{12}Asp and do not seem to form fibrous assemblies. The 2-hydroxy group in C_{12}HAsp can freely rotate, whereas the amide group in C_nAsp is in the planar trans configuration. The lack of a rigid group and the decreased hydrogen-bonding ability in a C_{12}HAsp molecule may cause the insolubility in water and the lack of formation of vesicles and fibers.

Formation of Molecular Assemblies by C_{12}Glu. A phase diagram for aqueous C_{12}Glu solutions of 1% is compared with that of C_{12}Asp in Figure 8. Aqueous C_{12}Glu solutions are translucent and less viscous at low pH and high temperature. They continuously lose fluidity with decreasing temperature, resulting in gels without fluidity at lower temperatures. At pH values higher than for the gel region, the needle-like crystals precipitate in slightly viscous solutions at low temperature. Amorphous aggregates are observed in gels by optical microscopy, suggesting the difference in molecular assemblies in the gel region of C_{12}Glu and in the gel-like region of C_{12}Asp.

The electron micrograph using a negative staining method in Figure 9 was taken from C_{12}Glu gels of 1% at pH 4.64. Spherical

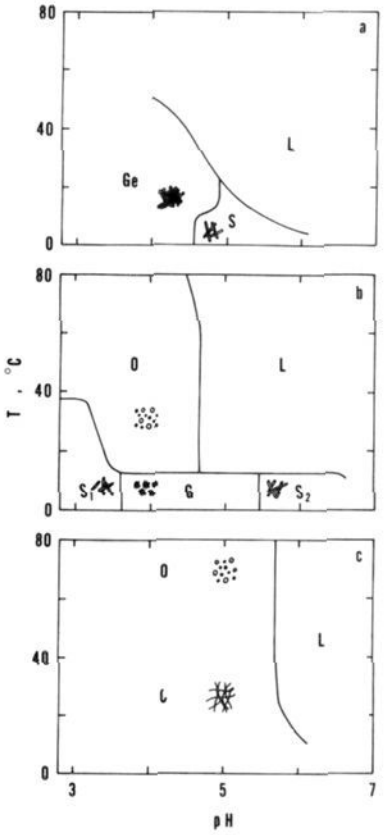

Figure 8. Temperature–pH phase diagrams for aqueous solutions of C_{12}Glu, C_{12}Asp, and C_{12}Ala of 1%: (a) C_{12}Glu; (b) C_{12}Asp; (c) C_{12}Ala. Notation: Ge, gel; C, cylindrical. The other signs have the same meaning as those in Figure 2. The images from optical microscopy are schematically drawn.

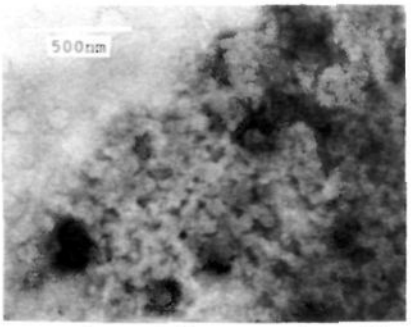

Figure 9. Electron micrograph from a negative staining method of C_{12}Glu gels of 1% at pH 4.64.

particles with diameters less than 100 nm coagulate to make gels. Since the images do not present any membrane layers, C_{12}Glu particles may be oil droplets rather than vesicles.

C_{12}Asp molecules are associated into fibrous assemblies but G_{12}Glu cannot be in spite of the similarity of their molecular structures and titration curves (Figure 1). Although the reason is now uncertain, it can be assumed that the longer side chain of glutamic acid may disturb the steric packing of head groups in the ordered assemblies. The other possibility is that the gel-liquid crystal phase transition temperature of aqueous C_{12}Glu solutions is higher than the temperature (90 °C) at which solutions are aged.

Formation of Molecular Assemblies by C_{12}Ala. Figure 8 includes the phase diagram for aqueous C_{12}Ala solutions. C_{12}Ala in water below pH 5.7 forms cylindrical fibers at low temperature, which are evidently visible with the optical microscope. They gradually disappear with increasing temperature, and opalescent solutions are obtained at high temperature. The existence of spherical particles in the opalescent solutions is ascertained by an optical microscope.

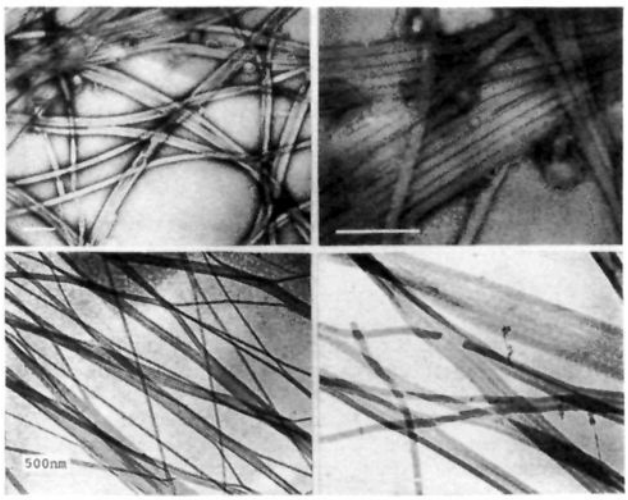

Figure 10. Electron micrographs of a C_{12}Ala solution of 1% at pH 5.2: upper, negative staining; lower, cryo. The bars represent 500 nm.

The electron micrographs for a C_{12}Ala solution of 1% at pH 5.2 reveal cylindrical images, as shown in Figure 10. The uniform, common diameter of cylindrical fibers, which is estimated from photographs taken using a cryo method, is about 40 nm. Cylindrical C_{12}Ala fibers are very long and more rigid than fibers in the gel-like C_nAsp solutions, depending on their thick diameter. They have no twisted or helical conformation, which is different from C_nAsp fibers. The C_{12}Ala fibers strongly contact in terms of the side-by-side interaction. The interacting strings make bundles or ribbons. As ribbons readily burst in one string, the burst string may constitute a part of another ribbon. Assembly formation by C_{12}Ala is compared with that of C_nAsp and C_{12}Glu in Table I.

Cylindrical assemblies can be formed by C_{12}Ala molecules because of the existence of the planar amide group. The formation of such assemblies is not suppressed by the lack of one of the branched dicarboxyl groups, but seems to be rather promoted by the linear hydrophilic chain in a C_{12}Ala molecule. It is worth noting that C_{12}Ala molecules are without asymmetric carbon and cannot form the helical structure.

Experimental Section

Materials. C_nAsp, C_{12}Glu, and C_{12}Ala were synthesized from alkanoyl chlorides and L-amino acids by the Schotten–Bouman method. The synthesis of C_{12}HAsp was in accordance with Patent No. JP48056381. All samples were kindly supplied by Mitsubishi Petrochemical Co., Ltd., Japan. The purity of C_nAsp (n = 10–18) was determined by high-performance liquid chromatography (HPLC) and nitrogen quantitative analysis as follows: C_{10}Asp, 98%; C_{12}Asp, 95%; C_{14}Asp, 92%; C_{16}Asp, 92%; C_{18}Asp, 89%.

Water was redistilled from alkaline $KMnO_4$ and boiled for 1 h. Standardized solutions of HCl and NaOH are commercial products.

pH Titration. The pH titration was performed at room temperature on an Iwaki Glass pH/ion meter A-225 under nitrogen atmosphere. The degree of ionization, α, is calculated by

$$\alpha = 1 - (C_{H^+,total} - C_{H^+,free})/2C \quad (1)$$

where $C_{H^+,total}$ and $C_{H^+,free}$ are the added total and free molar amounts of hydrogen ions, respectively, and C represents the molar amount of surfactant. Aqueous solutions were prepared by adding an adequate amount of HCl or NaOH to aqueous surfactant solutions which were neutralized beforehand by equivalent NaOH. Each solution was stored overnight before the pH measurement.

Phase Diagram. Surfactants were mixed in water with an adequate amount of standardized NaOH solution, and the mixtures were heated to 80–90 °C. As surfactant solids dissolved, the solutions were maintained at the desired temperature in a water bath. After 2 h, the occurrence of precipitates, opalescence, and so forth was inspected visually and by using an Olympus BH optical microscope equipped with a thermojacket. The temperature of the solution was then lowered and the same procedure was repeated. The pH measurement was performed for solutions which were again incubated at 25 °C.

Electron Microscopy. Transmission electron microscopic (TEM) observation was carried out at room temperature on a Hitachi H-800 electron microscope, operated at 100 or 200 kV. Negative staining, cryo, and freeze–fracture methods were utilized. For the negative staining method, the dried specimen on a carbon-coated electron microscope grid was negatively stained with 1% uranyl acetate solution.

The cryo–TEM observation was performed according to a procedure in the literature.[30] A filmy drop of surfactant solution on an electron microscope grid was vitrified by jet-freezing in cooled liquid ethane. A grid with the vitrified specimen was mounted on a Hitachi H5001-C cold stage and supplied to the TEM observation under liquid N_2 cooling.

The freeze–fracture replica film was prepared on a Balzers BAF 400 freeze–fracture device as follows: an aliquot of surfactant solution on a sample stage was vitrified in cooled liquid freon. Under reduced pressure, the vitrified specimen was fractured at −130 °C, and the fractured surface was shadowed by platinum at an elevation angle of 45° and deposited by carbon at 90°. The replica film was washed with sodium hypochloride solution and water.

Rheology. The rheology measurement was carried out at 25 °C on a Rheology Engineering MR-3 rheometer.

Infrared Spectra. The gel-like solution was mounted on a KRS-5 window, and the solvent was quickly vaporized in air. Infrared spectra for dried specimens on KRS-5 were recorded at room temperature by a JASCO IRA-2 diffraction grating infrared spectrophotometer.

Acknowledgment. We are grateful to Prof. Y. Talmon, Technion-Israel Institute of Technology, and Dr. P. Vinson, University of Minnesota, for their technical suggestions on electron microscopic observation. We also thank Mr. K. Hanaichi, Mr. T. Iwamoto, and Mr. N. Yokoi, Nagoya University, for their help with the electron microscopic observations.

Registry No. C_{10}Asp, 1116-12-7; C_{12}Asp, 1116-14-9; C_{16}Asp, 1782-17-8; C_{18}Asp, 1116-15-0; C_{12}HAsp, 139731-51-4; C_{12}Glu, 3397-65-7; C_{12}Ala, 21539-56-0.

(30) Bellare, J. R.; Davis, H. T.; Scriven, L. E.; Talmon, Y. *J. Electron Microsc. Tech.* **1988**, *10*, 87–111.